

Flux-Driven Conductance Scaling in Disordered Topological Insulator Nanowires

Shimon Arie Haver, Emuna Rimón, and Eytan Grosfeld*

Department of Physics, Ben-Gurion University of the Negev, Be'er-Sheva 84105, Israel

(Dated: February 25, 2026)

We study quantum transport in disordered topological insulator nanowires (TINWs) under axial magnetic flux. At integer flux quanta, spin–momentum locking produces weak anti-localization peaks, while at half-integer flux quanta a helical mode protected by time-reversal symmetry (TRS) suppresses backscattering. By analyzing the flux dependence of the localization length, we uncover critical scaling around half-integer flux quanta, reflecting the competition between disorder scattering and flux-induced breaking of TRS protection. As the disorder strength increases, we identify a crossover in scaling behavior that drives the system into a regime governed by a universal critical exponent. Our results demonstrate a scaling collapse across flux values, establishing a universal regime of flux-driven delocalization in TINWs.

Introduction.— Quantum transport in topological insulator nanowires (TINWs) offers a powerful platform to explore the interplay between topology, dimensionality, and disorder. Their low-energy physics is governed by a single-node massless Dirac equation constrained to the wire’s surface. When subjected to an axial magnetic field, TINWs display rich flux-dependent phenomena arising from the unique properties of their surface-state band structure [1, 2]. Recent progress in fabricating bulk-insulating nanowires [3] has further enhanced the feasibility of probing these effects experimentally.

A hallmark of this system is the appearance of weak anti-localization (WAL) peaks in the conductance at integer flux quanta, a consequence of spin–momentum locking and quantum interference [4]. At half-integer flux quanta, the surface states host a topologically protected helical mode that remains immune to non-magnetic backscattering due to time-reversal symmetry (TRS), leading to a distinctive conductance peak. Together, these mechanisms reshape the periodicity of Aharonov–Bohm oscillations [2, 5–9].

The axial flux thus provides a natural tuning knob that modulates transport and drives crossovers between localized and delocalized regimes [7]. The key quantity governing this behavior is the localization length, which controls the decay of conductance with wire length.

In this work, we investigate the dependence of the localization length in TINWs on axial flux and disorder. Near half a flux quantum, where a perfectly transmitting mode emerges, we demonstrate critical scaling governed by a universal exponent. Strikingly, this exponent assumes two distinct values depending on the chemical potential: at low chemical potentials it reflects the competition between disorder scattering and flux-induced breaking of TRS protection, while at higher chemical potentials it captures the residual ballistic character of the protected mode. By further increasing the disorder strength, we reveal a crossover in the scaling behavior, marking the onset of a universal regime characterized by a critical exponent of the flux-driven delocalization transition in TINWs.

Scaling of conductance with wire length.— We consider the TINW’s surface hamiltonian $\hat{H}_{\text{nw}} + \hat{V}$, with $\hat{H}_{\text{nw}} = \hbar\Omega \left[\sigma_z \left(\hat{\ell} + \frac{1}{2} - \eta \right) - \sigma_y \hat{k} R \right]$ and $\hat{V} = V(z, \varphi) \sigma_0$ the disorder potential. Here, σ_j ($j = x, y, z$) are the Pauli matrices in the spin-basis and σ_0 the 2×2 identity matrix; $\hat{k} = -i\partial_z$ and $\hat{\ell} = -i\partial_\varphi$ are proportional to the momentum and orbital angular momentum along the TINW, respectively; $\eta = \Phi/\Phi_0$ is the dimensionless flux (with $\Phi_0 = h/e$); and, $\Omega = v_F/R$ is the angular frequency associated with the electron motion around the circumference of the TINW with R its radius and v_F its Fermi velocity. [10] We consider multiple impurities at z_s , $s = 1, \dots, N$, described by the separable potential $V(z, \varphi) = \sum_s V_s Z(z - z_s) Y(\varphi)$, expanding the angular part $Y(\varphi) = 2 \sum_{m \in \mathbb{Z}} Y_m e^{im\varphi}$ with $Y_{-m} = Y_m^*$. We find the scattering state at energy E , $\Psi_E(z, \varphi)$, by employing a scattering matrix approach (described under Methods below) to compute the conductance as a function of the length of the wire traversed by the electrons. We averaged 1000 realizations with V_s , the amplitude of the scattering potential in the scatterer s , uniformly distributed

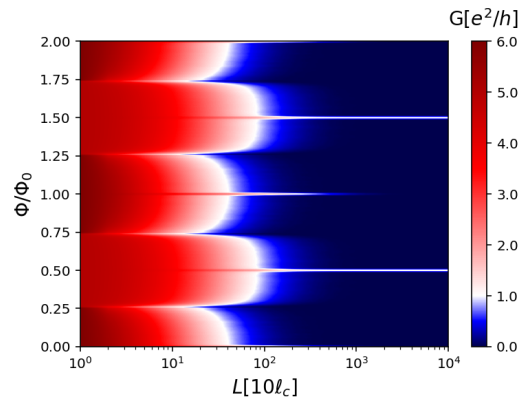


FIG. 1. **Variation of the conductance with the wire length and the dimensionless axial flux.** With $\mu[\hbar\Omega] = 2.751$, 5-6 channels participate in the conductance, depending on Φ/Φ_0 . $R[10^3\ell_c] = 0.2$ and the disorder strength is $W = 0.05$. The results are averaged over 1000 realizations.

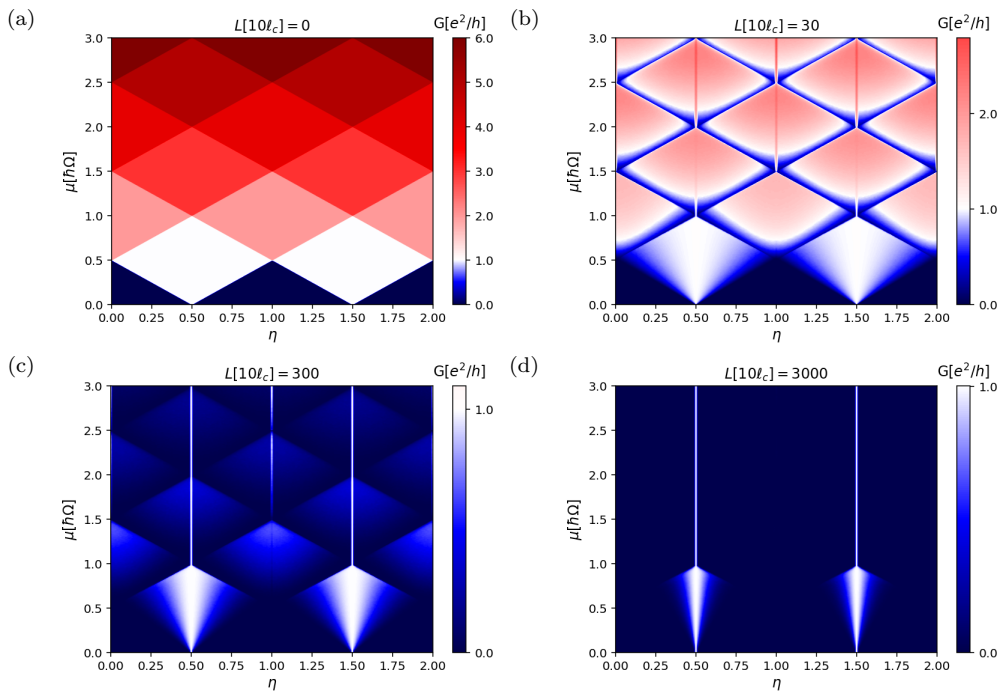


FIG. 2. **Variation of the conductance with the chemical potential and the dimensionless axial flux**, for wire lengths $L[10\ell_c] = 0$ (a), 30 (b), 300 (c), and 3000 (d). The diamond pattern in the clean limit transitions as L increases into a sharp peak at $\eta = 1/2$, where the helical state persists; while the weak anti-localization peak remains visible at $\eta = 1$ for moderate system lengths. The parameters are the same as in Fig. 1.

over $[-W, W]$, and $Y_m = 1$ for all m . The positions of the scatterers along z are taken to be randomly distributed, with a mean spacing ℓ_c .

Setting the chemical potential constant and modulating the axial magnetic flux, the number of conducting channels, $n = \ell_{\max} - \ell_{\min} + 1$, with $\ell_{\min} = \lceil -\tilde{\mu} - \frac{1}{2} + \eta \rceil$ and $\ell_{\max} = \lfloor \tilde{\mu} - \frac{1}{2} + \eta \rfloor$, alternates between n_0 and $n_0 + 1$. In addition, we included evanescent states in the calculation; because only those states that lie very close to the chemical potential have a significant effect, we limited the analysis to the four lowest-lying evanescent modes. As the TINW's length increases, the disorder starts to dominate, and eventually most of the values of the magnetic field lead to full localization except sharply at half flux quantum where the helical state remains fully conducting for arbitrary system size (Fig. 1). This perfectly transmitted mode arises from the odd number of channels, preserved by the system's time-reversal invariance [2, 11]. Additionally, at integer flux quanta where the system remains time-reversal invariant one can observe the WAL peaks at intermediate lengths. They eventually localize as the system crosses to the strongly-localized regime.

The dependence on chemical potential is explored in Fig. 2. The observed diamond pattern is related to the opening and closing of conduction channels in the clean limit. Although at higher chemical potential the ballistic conductance is greater, it decays more strongly with dis-

order. Consequently, even for short L , there is no longer a significant difference between the diamonds containing different numbers of conducting modes. The remaining dependence on the chemical potential is mostly due to the van-Hove singularity near the edges of the diamonds, where the density of states is diverging. In contrast, in the regime where only a single conducting mode exists (at low chemical potentials), the decay is the slowest. For longer wires, the ballistic diamond pattern evolves to WAL peaks and peaks associated with the helical channel at integer and half-integer flux quantum. Finally, only the helical channel peaks survive.

The WAL peaks increase as the chemical potential shifts away from the Dirac point. The usual picture for the WAL involves scattering between $\mathbf{k} = (k, \ell)$ states along the fermi surface until it eventually returns to the initial \mathbf{k} . Due to the presence of the Dirac point, the system acquires a π Berry phase through these multiple scattering events. This process results in destructive interference at zero magnetic field, which increases the conductance. Close to the Dirac point, the system explores a discrete version of this WAL mechanism, with only a finite number of states available for this scattering at low $\tilde{\mu}$. The number of available conduction channels increases with $\tilde{\mu}$, and so does the strength of the WAL peaks, as we can see in Fig. 3. At $\tilde{\mu} = m + 1/2$ with $m \in \mathbb{Z}$ the WAL peak gets suppressed due to the van-Hove singularity. While the behavior changes significantly for small

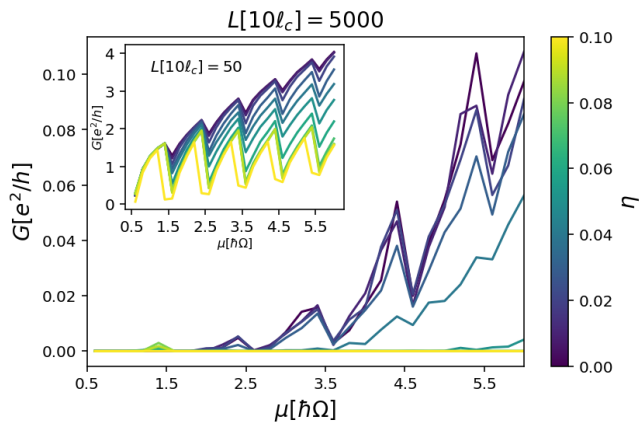


FIG. 3. Variation of the weak anti-localization peaks with the chemical potential, at zero flux, for wire length $L[10\ell_c] = 5000$ ($L[10\ell_c] = 50$ in the inset). The parameters are the same as in Fig. 1.

μ , the WAL peaks remain visible also with a low number of scattering channels, disappearing when we have only two open channels.

Critical exponent around delocalization point.—

The scaling theory of localization provides a framework for understanding how the conductance of a disordered electronic system changes with system size and how it transitions between metallic and insulating phases [12–16]. In our case, while the conductance remains non-zero only at half-flux in the infinite-system limit, the localization length describing its decay remains finite, diverging towards half-flux as a power law. To extract the critical exponent, we relate the localization length at length L of the wire to the conductance at length L , G_L , via $\xi_L = -L/\log(G_L/G_0)$. The thermodynamic ($L \rightarrow \infty$) behavior is extracted using a scaling argument [17, 18]. It is assumed that $\xi_L(\eta)$ and $\xi(\eta) = \lim_{L \rightarrow \infty} \xi_L(\eta)$ are related by a universal function that does not depend on the dimensionless flux η or the length L separately,

$$\xi_L(\eta)/L = F[\xi(\eta)/L]. \quad (1)$$

Its form is extracted in Fig. 4a using a numerical procedure [19]. In the limit $L \rightarrow \infty$, the argument of F becomes small, while Eq. 1 indicates that $F(x)$ becomes a linear function, $F(x) \simeq x$. In the opposite limit $L \ll \xi(\eta)$, the correlation length is limited by the size of the system, leading to $\xi_L(\eta) \sim L$ or $F(x) \rightarrow F_0$ for large x , where F_0 is a constant. At criticality at $\eta = 1/2$, the state is extended to $\xi(1/2) = \infty$, and hence the scaling equation predicts $\xi_L(1/2) = F_0 L$. In addition, the conductance $\lim_{L \rightarrow \infty} \tilde{G}_L \rightarrow 1$ (with $\tilde{G}_L = G_L/(e^2/h)$, the unitless conductance) hence $\lim_{L \rightarrow \infty} \xi_L(1/2)/L = \log(\tilde{G}_0)^{-1}$ so the value of the constant is set by the ballistic conductance, $F_0 = \log(\tilde{G}_0)^{-1}$. This linear relation between $\xi_L(1/2)$ and L only holds asymptotically for large enough L . For nearby values of flux, the system is ballistic for

$L \rightarrow 0$, $\tilde{G}_L = n$, the number of open channels, then goes through a diffusive regime with WAL corrections and corrections due to the ballistic channel, finally reaching the localized regime for large enough L such that $\tilde{G}_L < 1$ (the regime when $\xi_L(\eta) < \xi_L(1/2)$ for all $\eta \neq 1/2$). The resulting $\xi(\eta)$ is displayed as a function of η in Fig. 4, and is demonstrated to diverge as a power law at half a quantum flux through the TINW, $\xi(\eta) \sim |\eta - 1/2|^{-\nu}$.

Calculating the localization length over a wide range of disorder values, from $W = 0.01$ to $W = 10$, it is demonstrated that for large enough disorder ($W > 0.1$), the localization length does not depend on the disorder strength. This leads to the saturation of ν in the inset of Fig. 4b, which achieves the value $\nu = 1.7 \pm 0.1$.

A dimensional crossover is driven by the chemical potential: for lower chemical potentials, for which only a single conducting channel is available, the system is rendered effectively one-dimensional. The observed localization away from $\eta = 1/2$ stems from the generation of a gap which allows for backscattering. The observed critical exponent of $\nu = 2$ near $\eta = 1/2$ saturates the Harris criterion in one dimension. For higher values of the chemical potential, multiple channels become accessible, and the system crosses into two-dimensional behavior. Fig. 4b displays the critical exponent ν as a function of the disorder strength, W .

Methods.— We now describe the formalism we use for the numerical extraction of the conductance. In a sense, this reduces the quasi-one dimensional problem to a disordered Kronig-Penney model [20] with scattering between the channels. This allows for the extraction of the transport properties over large system sizes.

For a single scatterer at $z = z_s$, we write the states at energy $\mu > 0$ on the two sides of the scatterer

$$\begin{aligned} |\Psi_\mu(z < z_s, \varphi)\rangle &= \sum_{\ell, \alpha} a_\ell^\alpha e^{i\alpha k_\ell z} e^{i\ell\varphi} |\Psi_{\ell\alpha}\rangle, \\ |\Psi_\mu(z > z_s, \varphi)\rangle &= \sum_{\ell, \alpha} b_\ell^\alpha e^{i\alpha k_\ell z} e^{i\ell\varphi} |\Psi_{\ell\alpha}\rangle. \end{aligned} \quad (2)$$

Here a_ℓ^α and b_ℓ^α are the amplitudes associated with the orbital ($\ell \in \mathbb{Z}$) and linear momentum (αk_ℓ) mode along the z -direction, with $k_\ell > 0$ and $\alpha = \pm$ denoting a right/left mover. Here k_ℓ is taken on the Fermi surface and is the positive root of $\tilde{\mu} = \sqrt{(\ell + \frac{1}{2} - \eta)^2 + \tilde{k}_\ell^2}$. The spinors can be written as $|\Psi_{\ell\alpha}\rangle = U_{\ell\alpha}^\dagger |+\rangle$ with $U_{\ell\alpha} = \frac{1}{\sqrt{k_\ell}} \exp(i\frac{1}{2}\sigma_x \theta_{\ell\alpha})$ and $\theta_{\ell\alpha} = \arctan\left(\ell + \frac{1}{2} - \eta, \alpha \tilde{k}_\ell\right)$. Here $\arctan(x, y)$ is the four-quadrant inverse tangent and $|+\rangle = (1, 0)^T$. The states are normalized by the group velocity $v(k_\ell) \propto k_\ell$ to ensure that each mode carries the same probability flux as required by transport calculations [21].

Taking a separable potential $V(z, \varphi) = V_s Z(z) Y(\varphi)$, expanding $Y(\varphi) = 2 \sum_{m \in \mathbb{Z}} Y_m e^{im\varphi}$ with $Y_{-m} = Y_m^*$ and $Z(z) = \hbar\Omega R\delta(z)$, and integrating the Dirac equation

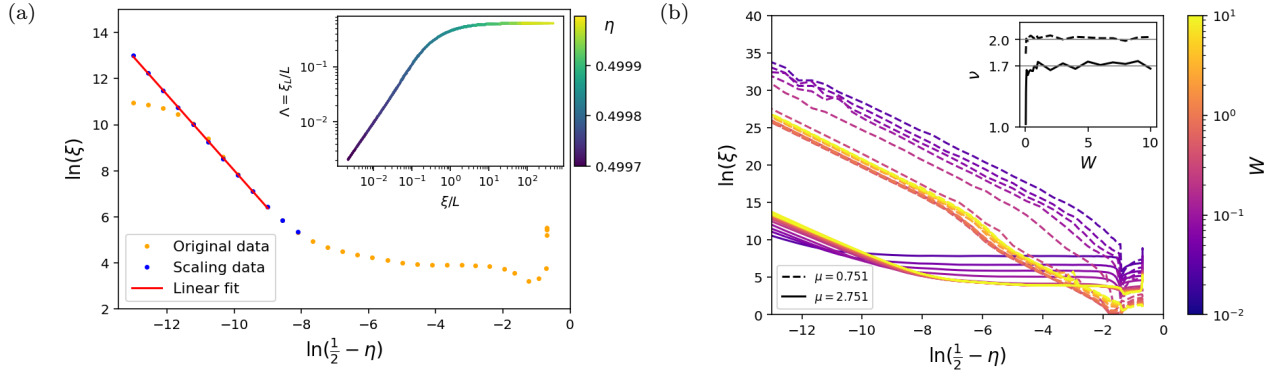


FIG. 4. **Delocalization transition near half-flux quantum**, $\eta = 1/2$. (a) The raw ξ_L for $L = 10^5 \ell_c$ and $\mu[\hbar\Omega] = 2.751$ (orange), and rescaled localization length ξ (blue) as function of $1/2 - \eta$. A linear fit to the rescaled data (red) in the scaling regime gives a critical exponent of $\nu = 1.64$, near $\eta = \Phi/\Phi_0 = 1/2$. The inset shows the collapse to a universal function of ξ_L/L as a function of ξ/L for different flux values. (b) The localization length ξ as function of $1/2 - \eta$, for two values of μ ($\mu[\hbar\Omega] = 0.751, 2.751$) and several disorder strengths. In the inset, the critical exponent ν is displayed as function of the disorder strength. For $W > 0.1$, the critical exponents are $\nu = 2.02 \pm 0.03$, and $\nu = 1.7 \pm 0.1$ respectively.

around the impurity, we get

$$i\sigma_y (|\Psi(z_s^+, \varphi)\rangle - |\Psi(z_s^-, \varphi)\rangle) + V_s \sum_m Y_m e^{im\varphi} (|\Psi(z_s^+, \varphi)\rangle + |\Psi(z_s^-, \varphi)\rangle) = 0. \quad (3)$$

Substituting Eq. (2), the equation assumes the form

$$\sum_{\ell\alpha} \left[i\sigma_y (b_\ell^\alpha - a_\ell^\alpha) + V_s \sum_m Y_m e^{im\varphi} (b_\ell^\alpha + a_\ell^\alpha) \right] e^{i\ell\varphi} |\Psi_{\ell\alpha}\rangle = 0. \quad (4)$$

We next project on the basis elements, by multiplying from the left by $\langle \Psi_{\ell'\alpha'} | e^{-i\ell'\varphi}$, then averaging the equation over angles, $\frac{1}{2\pi} \int_0^{2\pi} d\varphi$,

$$\sum_{\ell\alpha} \left(\mathcal{Y}_{\ell'\alpha';\ell,\alpha} \delta_{\ell',\ell} + V_s \sum_m \mathcal{V}_{\ell'\alpha';\ell\alpha}^{(m)} \delta_{\ell'-m,\ell} \right) b_\ell^\alpha = \sum_{\ell\alpha} \left(\mathcal{Y}_{\ell'\alpha';\ell\alpha} \delta_{\ell',\ell} - V_s \sum_m \mathcal{V}_{\ell'\alpha';\ell\alpha}^{(m)} \delta_{\ell'-m,\ell} \right) a_\ell^\alpha, \quad (5)$$

where we defined

$$\mathcal{V}_{\ell'\alpha';\ell\alpha}^{(m)} = Y_m \langle \Psi_{\ell'\alpha'} | \Psi_{\ell\alpha} \rangle = \frac{Y_m}{\sqrt{k_{\ell'} k_\ell}} \cos\left(\frac{\theta_{\ell'\alpha'} - \theta_{\ell\alpha}}{2}\right),$$

$$\mathcal{Y}_{\ell'\alpha';\ell\alpha} = i \langle \Psi_{\ell'\alpha'} | \sigma_y | \Psi_{\ell\alpha} \rangle = \frac{-i}{\sqrt{k_{\ell'} k_\ell}} \sin\left(\frac{\theta_{\ell'\alpha'} + \theta_{\ell\alpha}}{2}\right).$$

The matrix elements satisfy: $\mathcal{V}_{\ell'\alpha';\ell\alpha}^{(m)*} = \mathcal{V}_{\ell\alpha;\ell'\alpha'}^{(-m)}$ and $\mathcal{Y}_{\ell'\alpha';\ell\alpha}^* = -\mathcal{Y}_{\ell\alpha;\ell'\alpha'}$. For ℓ, ℓ' that satisfy $\ell + \frac{1}{2} - \eta = -(\ell' + \frac{1}{2} - \eta)$ we have no backscattering $\mathcal{V}_{\ell'\alpha';\ell,-\alpha}^{(m)} = 0$. Also, generally, $\mathcal{Y}_{\ell\alpha;\ell,-\alpha} = 0$.

From this equation, we can extract the transfer matrix M [22], $\mathbf{b} = M_s \mathbf{a}$, which relates the amplitudes to the left

of the impurity $\mathbf{a} = (a^+, a^-)^T$ and those to the right of the impurity, $\mathbf{b} = (b^+, b^-)^T$. Here a^α (b^α) are row vectors whose elements are the set a_ℓ^α (b_ℓ^α) for all allowed ℓ 's, e.g., $a^\alpha = (a_{\ell_{\min}}^\alpha, \dots, a_{\ell_{\max}}^\alpha)$. Equivalently, we can write the scattering matrix $S_s = \begin{pmatrix} r_s & t'_s \\ t_s & r'_s \end{pmatrix}$, written in terms of the reflection matrices r_s and r'_s (reflection from left to left and from right to right) and transmission matrices t_s and t'_s (transmission from left to right and from right to left), $\mathbf{c}^{\text{out}} = S_s \mathbf{c}^{\text{in}}$, where $\mathbf{c}^{\text{in}} = (a^+, b^-)^T$ and $\mathbf{c}^{\text{out}} = (a^-, b^+)^T$. The transfer matrix can be written in terms of the submatrices of the scattering matrix as follows,

$$M_s = \begin{pmatrix} (t'_s)_{-1}^{-1} & r'_s t'_s{}^{-1} \\ -t'_s{}^{-1} r_s & t'_s{}^{-1} \end{pmatrix}.$$

For the case of multiple impurities, $s = 1, \dots, N$, we describe a system of a conductor with defects so that the electron propagates freely from one defect to the next. The transfer matrix encapsulates the process of multiple scatterings, $\mathcal{M}_N = \prod_{s=N}^1 M_s \tilde{M}_s$. Here M_s is the transfer matrix for impurity s , extracted from Eq. 5; and, \tilde{M}_s is the transfer matrix for the clean translation over distance $\Delta z_s = z_s - z_{s-1}$ between scatterers $s-1$ and s (with $z_0 = 0$ and $z_N = L$), obtained from M_s by the replacements $t_s, t'_s \rightarrow \exp(iK\Delta z_s)$ and $r_s, r'_s \rightarrow 0$, with $K = \text{diag}(k_{\ell_{\min}}, \dots, k_{\ell_{\max}})$. Due to the exponentially large and small eigenvalues of the transfer matrix, the matrix product is numerically unstable [23, 24]. So, instead, we work with the scattering matrix. Multiple scatterings are described via $\mathcal{S}_N = \bigotimes_{s=N}^1 S_s \otimes \tilde{S}_s$, where \tilde{S}_s is associated with the translation between two scatterers and is obtained from S_s using the same prescription

as in the M -matrix, while [23, 24]

$$S_2 \otimes S_1 \equiv \begin{pmatrix} r_1 + t'_1 r_2 (1 - r'_1 r_2)^{-1} t_1 & t'_1 (1 - r_2 r'_1)^{-1} t'_2 \\ t_2 (1 - r'_1 r_2)^{-1} t_1 & r'_2 + t_2 r'_1 (1 - r_2 r'_1)^{-1} t'_2 \end{pmatrix}. \quad (6)$$

The conductance is given by the Landauer formula $G = \frac{e^2}{h} \text{Tr}(t^\dagger t)$, where t is the total transmission matrix extracted from \mathcal{S}_N .

In addition to the propagating states, for which $k_\ell \in \mathbb{R}$, we can also include evanescent states [25, 26], for which $k_\ell = i\kappa_\ell$ and $\Psi_\mu(z, \varphi) \sim e^{-\kappa_\ell z}$, in the calculation. These states are excluded from the final computation of the transmission and reflection matrices, as they do not carry current, but they affect the transmission and reflection coefficients of the propagating states. The primary effect of these states becomes significant only when the chemical potential is close enough to the bottom of an excited subband, otherwise, they decay too rapidly to have a noticeable influence [23].

Conclusions.— We demonstrated how the conductance of a topological insulator nanowire (TINW) scales with the nanowire length in the presence of disorder. Furthermore, we analyzed its behavior as a function of the magnetic flux and chemical potential, providing insights into the interplay between WAL and helical modes. Our central result is the extraction of the localization length ξ as a function of the dimensionless flux, η , and the identification of the associated critical scaling exponent, highlighting the universality of the delocalization transition.

Other sources of disorder in TINWs include magnetic impurities, which break time-reversal symmetry and can localize the helical surface states, thereby suppressing the characteristic anti-localization response. In addition, local curvature or geometric inhomogeneities [24] can generate quasi-bound states that further enhance localization tendencies [27]. These effects highlight intriguing directions for future studies of disorder-driven localization in topological nanowires. Beyond their fundamental relevance, our results may also provide useful guidance for the implementation of TINWs in gatemon-type superconducting devices [28, 29], where understanding the interplay between disorder, topology, and superconducting proximity is essential.

We are grateful to D. Dahan for useful discussions. We would like to thank the Israeli Ministry of Innovation, Science and Technology for support under the UK/Israel Research Collaboration Grant QuantumGate.

* grosfeld@bgu.ac.il

[1] P. M. Ostrovsky, I. V. Gornyi, and A. D. Mirlin, Interaction-induced criticality in \mathbb{Z}_2 topological insulators, *Phys. Rev. Lett.* **105**, 036803 (2010).

- [2] J. H. Bardarson and J. E. Moore, Quantum interference and aharonov–bohm oscillations in topological insulators, *Reports on Progress in Physics* **76**, 056501 (2013).
- [3] M. Rossler, D. Fan, F. Munning, H. F. Legg, A. Bliesener, G. Lippertz, A. Uday, R. Yazdanpanah, J. Feng, A. Taskin, *et al.*, Top-down fabrication of bulk-insulating topological insulator nanowires for quantum devices, *Nano Letters* **23**, 2846 (2023).
- [4] S. Hikami, A. I. Larkin, and Y. Nagaoka, Spin-orbit interaction and magnetoresistance in the two dimensional random system, *Progress of Theoretical Physics* **63**, 707 (1980).
- [5] J. H. Bardarson, P. W. Brouwer, and J. E. Moore, Aharonov-bohm oscillations in disordered topological insulator nanowires, *Phys. Rev. Lett.* **105**, 156803 (2010).
- [6] Y. Zhang and A. Vishwanath, Anomalous aharonov-bohm conductance oscillations from topological insulator surface states, *Phys. Rev. Lett.* **105**, 206601 (2010).
- [7] S. Cho, B. Dellabetta, R. Zhong, J. Schneeloch, T. Liu, G. Gu, M. J. Gilbert, and N. Mason, Aharonov–bohm oscillations in a quasi-ballistic three-dimensional topological insulator nanowire, *Nature Communications* **6**, 7634 (2015).
- [8] L. A. Jauregui, M. T. Pettes, L. P. Rokhinson, L. Shi, and Y. P. Chen, Magnetic field-induced helical mode and topological transitions in a topological insulator nanoribbon, *Nature Nanotechnology* **11**, 345 (2016).
- [9] F. Munning, O. Breunig, H. F. Legg, S. Roitsch, D. Fan, M. Rößler, A. Rosch, and Y. Ando, Quantum confinement of the dirac surface states in topological-insulator nanowires, *Nature communications* **12**, 1038 (2021).
- [10] S. A. Haver, E. Ginossar, S. E. de Graaf, and E. Grosfeld, Electromagnetic response of the surface states of a topological insulator nanowire embedded within a resonator, *Communications Physics* **6**, 101 (2023).
- [11] T. Ando and H. Suzuura, Presence of perfectly conducting channel in metallic carbon nanotubes, *Journal of the Physical Society of Japan* **71**, 2753 (2002).
- [12] J. Edwards and D. Thouless, Numerical studies of localization in disordered systems, *Journal of Physics C: Solid State Physics* **5**, 807 (1972).
- [13] D. J. Thouless, Electrons in disordered systems and the theory of localization, *Physics Reports* **13**, 93 (1974).
- [14] D. Licciardello and D. Thouless, Conductivity and mobility edges for two-dimensional disordered systems, *Journal of Physics C: Solid State Physics* **8**, 4157 (1975).
- [15] F. J. Wegner, Electrons in disordered systems. scaling near the mobility edge, *Zeitschrift für Physik B Condensed Matter* **25**, 327 (1976).
- [16] E. Abrahams, P. W. Anderson, D. C. Licciardello, and T. V. Ramakrishnan, Scaling theory of localization: Absence of quantum diffusion in two dimensions, *Phys. Rev. Lett.* **42**, 673 (1979).
- [17] J.-L. Pichard and G. Sarma, Finite size scaling approach to anderson localisation, *Journal of Physics C: Solid State Physics* **14**, L127 (1981).
- [18] J.-L. Pichard and G. Sarma, Finite-size scaling approach to anderson localisation. ii. quantitative analysis and new results, *Journal of Physics C: Solid State Physics* **14**, L617 (1981).
- [19] A. MacKinnon and B. Kramer, The scaling theory of electrons in disordered solids: Additional numerical results, *Zeitschrift für Physik B Condensed Matter* **53**, 1 (1983).
- [20] A. Sánchez, E. Maciá, and F. Domínguez-Adame, Sup-

- pression of localization in kronig-penney models with correlated disorder, *Phys. Rev. B* **49**, 147 (1994).
- [21] H. Bruus and K. Flensberg, *Many-body quantum theory in condensed matter physics: an introduction* (Oxford university press, 2004).
- [22] C. W. J. Beenakker, Random-matrix theory of quantum transport, *Rev. Mod. Phys.* **69**, 731 (1997).
- [23] H. Tamura and T. Ando, Conductance fluctuations in quantum wires, *Phys. Rev. B* **44**, 1792 (1991).
- [24] J. H. Bardarson and R. Ilan, Transport in topological insulator nanowires, in *Topological Matter: Lectures from the Topological Matter School 2017*, edited by D. Bercioux, J. Cayssol, M. G. Vergniory, and M. Reyes Calvo (Springer International Publishing, Cham, 2018) pp. 93–114.
- [25] M. Cahay, S. Bandyopadhyay, M. Osman, and H. Grubin, Influence of evanescent states on quantum transport through an array of elastic scatterers, *Surface Science* **228**, 301 (1990).
- [26] S. Bandyopadhyay, M. Cahay, D. Berman, and B. Nayfeh, The role of evanescent states in quantum transport through disordered mesoscopic structures, *Superlattices and Microstructures* **10**, 327 (1991).
- [27] R. Saxena, E. Grosfeld, S. E de Graaf, T. Lindstrom, F. Lombardi, O. Deb, and E. Ginossar, Electronic confinement of surface states in a topological insulator nanowire, *Phys. Rev. B* **106**, 035407 (2022).
- [28] K. Yavilberg, E. Ginossar, and E. Grosfeld, Differentiating majorana from andreev bound states in a superconducting circuit, *Physical Review B* **100**, 241408 (2019).
- [29] T. W. Schmitt, M. R. Connolly, M. Schleenvoigt, C. Liu, O. Kennedy, J. M. Chávez-García, A. R. Jalil, B. Benemann, S. Trellenkamp, F. Lentz, *et al.*, Integration of topological insulator josephson junctions in superconducting qubit circuits, *Nano letters* **22**, 2595 (2022).